Journal of Biomolecular NMR, 4 (1994) 97–116
ESCOM

J-Bio NMR 156

Assessing glycosidic linkage flexibility: Conformational analysis of the repeating trisaccharide unit of *Aeromonas salmonicida*

Thomas Peters* and Thomas Weimar

Institute of Biophysical Chemistry, University of Frankfurt, Biocenter, N230, Marie-Curie-Strasse 9, D-60439 Frankfurt, Germany

Received 15 July 1993
Accepted 6 September 1993

Keywords: Glycosidic linkage flexibility; Branching in saccharides; 1D NOE curves; Metropolis Monte Carlo simulations

SUMMARY

A detailed conformational analysis was performed for the synthetic branched trisaccharide β-D-ManNAc-(1→4)-[α-D-Glc-(1→3)]-L-Rha **1** which represents the repeating unit of the *O*-antigenic polysaccharide of *Aeromonas salmonicida*. The study was based on 26 experimental NOE curves from 1D transient NOE experiments, employing Gaussian-shaped inversion pulses at 600 MHz. Eight of the NOE curves were interglycosidic and thus useful for an analysis of glycosidic linkage orientations. Metropolis Monte Carlo (MMC) simulations and minimum-energy calculations with the program GEGOP were used to obtain theoretical NOE curves which were compared to the experimental ones. MMC simulations with different temperature parameters of 310, 600, 900 and 2000 K allowed identification of NOEs which are sensitive towards different conformation distributions – not only different conformations – at both glycosidic linkages in **1**. A comparison of trisaccharide **1** with the constituent disaccharides β-D-ManNAc-(1→4)-L-Rha **2** and α-D-Glc-(1→3)-L-Rha **3** revealed effects of branching on glycosidic linkage flexibility. A quantitative evaluation was facilitated by the introduction of entropy-related flexibility parameters. Our study indicates a notable restriction of flexibility, especially at the (1→3) linkage in **1**. Although overall flexibility in **1** is reduced as compared to the constituent disaccharides **2** and **3**, it cannot be neglected altogether. In summary, combined transient NOE experiments and MMC simulations provide a simple approach to analyse glycosidic linkage flexibility.

INTRODUCTION

During recent years there has been much debate whether glycosidic linkages are flexible or rigid (Cumming and Carver, 1987a,b; Ha et al., 1988; Imberty et al., 1989; Tran et al., 1989; Edge et al., 1990; Homans, 1990; Peters et al., 1990; Brady, 1991; Carver, 1991; Bock et al., 1992; Brisson et al., 1992; Bush, 1992; Homans and Foster, 1992; Poppe and Van Halbeek, 1992; Sabesan et al.,

*To whom correspondence should be addressed.

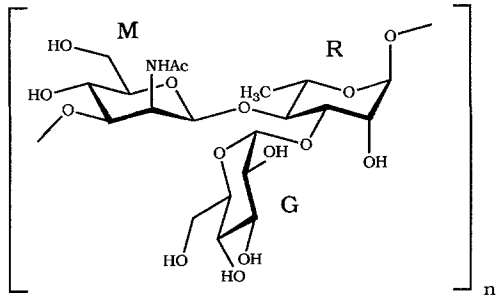

1 (n = 1)

1992; Peters et al., 1993) and recently, internal motions could be detected directly for two disaccharides using ^{1}H relaxation measurements (Hricovíni et al., 1992; Braccini et al., 1993). It is clear now that glycosidic linkage flexibility strongly depends on the type of glycosidic linkage and on branching patterns. Glycosidic linkages involving primary hydroxyl groups of side chains of pyranose rings, e.g. (1→6) linkages, are especially flexible but bonds to secondary hydroxyl groups still exhibit detectable flexibility (Cumming and Carver, 1987a,b). More rigid structures are found for branched saccharides such as the synthetic trisaccharide β-D-ManNAc-(1→4)-[α-D-Glc-(1→3)]-L-Rha **1** (Paulsen and Lorentzen, 1987) which represents the repeating unit (see scheme) of the antigenic polysaccharide of *Aeromonas salmonicida* (Shaw et al., 1983), a bacterium which causes furunculosis in salmon. Branched trisaccharides are also found as building blocks of blood-group antigens Le^a and Le^b and of the tissue antigenic determinant Le^x. Conformational analysis studies led to the conclusion that these structures are rather rigid (Thøgersen et al., 1982; Bechtel et al., 1990; Yan and Bush, 1990; Mukhopadhyay and Bush, 1991; Miller et al., 1992).

There have been only very few attempts to more precisely examine the conformational behaviour of glycosidic linkages on the basis of accurate NOE curves (Sabesan et al., 1992; Widmalm et al., 1992; Weimar et al., 1993). 1D or 2D NOESY experiments (Marion and Wüthrich, 1983; Kessler et al., 1986, 1991) may be performed for this purpose (Sabesan et al., 1992; Widmalm et al., 1992), but for molecules with small positive NOEs such as trisaccharide **1** it is more advantageous to use 1D transient NOE experiments with selective inversion of proton resonances (Neuhaus and Williamson, 1989). Compared to 1D and 2D NOESY experiments, these experiments provide a theoretical factor of two in intensity enhancement, while the buildup kinetics remain unaffected. This work describes the assessment of glycosidic linkage flexibility, based on high-accuracy 1D transient NOE curves and corresponding theoretical curves from Metropolis Monte Carlo (MMC) simulations (Levy et al., 1991; Poppe et al., 1992; Peters et al., 1993; Weimar et al., 1993), employing entropy-related flexibility parameters as a quantitative measure for the degree of flexibility.

Abbreviations: NOE, Nuclear Overhauser Effect; NOESY, Nuclear Overhauser Enhancement Spectroscopy; COSY, Correlation Spectroscopy; TOCSY, Total Correlation Spectroscopy; MMC, Metropolis Monte Carlo; GEGOP, Geometry of Glycoproteins; G, α-D-glucose; M, β-D-*N*-acetyl mannosamine; R, α-L-rhamnose; H2^M{H1^M}, NOE enhancement of H2^M upon selective inversion of H1^M.

MATERIALS AND METHODS

NMR experiments

β-D-ManNAc-(1→4)-[α-D-Glc-(1→3)]-L-Rha **1** was synthesized as described elsewhere (Paulsen and Lorentzen, 1987). Thirty mg of **1** was lyophilised twice from 1.0 ml D_2O (99.99%, MSD Isotopes) and then dissolved in 0.5 ml of D_2O (99.999%, MSD Isotopes). The sample was degassed by repeated evacuation and inflation with argon and was sealed under argon. For the measurement of the vicinal coupling constant $J_{NH,H2^M}$ the sample was dissolved in a mixture of 0.5 ml H_2O and 0.05 ml D_2O. All spectra were recorded on a Bruker AM 500 (500 MHz) or AMX 600 (600 MHz) spectrometer, equipped with an Aspect 3000 and an X32 computer, respectively. Proton chemical shifts are expressed relative to the HDO signal (4.72 ppm at 303 K), which sets the chemical shift for acetone at 2.22 ppm. All spectra were collected with 8K data points and were zero-filled to 16K prior to Fourier transformation. 1D ^1H NMR spectra were acquired at 303 K with a spectral width of 6 ppm.

1D transient NOE experiments were performed at 600 MHz at 310 K using relaxation delays of 4.5 s and 640 scans, preceded by 32 dummy scans each. Gaussian-shaped (Kessler et al., 1986) selective 180° pulses were used in these experiments. The 90° hard pulse was 13.6 μs. 2K data points were used to determine the shape of the Gaussian pulses with the truncation level set at 1%. Calibration of Gaussian pulses followed the protocol given by Kessler and co-workers (Kessler et al., 1986; Anders, 1989). The pulse lengths were chosen according to the width of the signals to be selectively excited. One set of experiments (inversion of $H1^M$, $H2^M$, $H5^M$ and $H3^R$) used an 80 ms (180°) pulse. Another set (inversion of $H2^R$) used a 400 ms (180°) pulse. Mixing times were corrected for the duration of the Gaussian pulses by adding half of the duration of the Gaussian pulses to the mixing time. Mixing times for the first set of experiments were: 41, 115, 220, 390, 540, 720, 940, 1140, 1340 and 1540 ms. Mixing times for the second set of experiments were: 201, 210, 250, 400, 550, 750, 950, 1150 and 1300 ms. Prior to the integration of signals, a third-order polynomial baseline correction was performed using UXNMR software. To obtain experimental NOEs, decaying signal intensities of selectively excited resonances were fitted towards a single exponential function $f(\tau_m) = C \exp(-\tau_m/T_{1sel})$, with C = scaling factor, τ_m = mixing time and T_{1sel} = selective spin-lattice relaxation time. Subsequently, all measured NOEs were scaled accordingly with the aid of a FORTRAN program employing the Levenberg–Marquardt algorithm (Press et al., 1986).

Phase-sensitive 2D NOESY and COSY experiments were performed at 500 MHz (315 and 300 K, respectively) using TPPI (Marion and Wüthrich, 1983). A phase-sensitive (TPPI) TOCSY experiment (Braunschweiler and Ernst, 1983; Bax and Davis, 1985; Davis and Bax, 1985) was performed also at 500 MHz (300 K) with the spectrometer operating in reverse mode. The MLEV-17 (Bax and Davis, 1985) spin-lock sequence embraced by trim pulses of 3 ms length was applied and a mixing time of 70 ms was used.

Calculations

All calculations were performed on Silicon Graphics 4D/35 or IBM-320 workstations. The calculation of the global minimum and the MMC simulations were performed with the program GEGOP (Stuike-Prill and Meyer, 1990). Coordinates for β-D-*N*-acetyl mannosamine were derived from neutron-diffraction data for α-D-mannose (Jeffrey et al., 1977), attaching the *N*-

acetyl group with standard geometry and setting the dihedral angle H2-C2-N-H at 178°. The latter is in accordance with that found for the orientation of the *N*-acetyl group in β-D-*N*-acetyl glucosamine (Winter et al., 1978) and was further validated by the measured value of the vicinal coupling constant $J_{NH,H2M}$ (10.0 Hz). In the case of X-ray data, hydrogen atoms were replaced with standard bond lengths (1.1 Å) and bond angles (109.5°). The pyranose rings were assumed to be rigid, residing either in the $^4C_1$ (residues G and M) or in the $^1C_4$ (residue R) conformation. Dihedral angles ϕ (H1'-C1'-O1'-Cx) and ψ (C1'-O1'-Cx-Hx) at glycosidic linkages and ω (O6-C6-C5-O5) at C5-C6 bonds were treated as flexible parameters with x being the aglyconic linkage site. Bond angles τ (C1'-O1'-Cx) at the glycosidic linkages were also considered to be flexible, applying a strong spring potential with an equilibrium value of 117° (Stuike-Prill and Meyer, 1990). MMC simulations were performed according to the protocol published recently (Peters et al., 1993; Weimar et al., 1993). Three sets of simulations were performed for the α-anomeric form of **1** with 10^6 macro steps each and temperature parameters set at 310, 600, 900 and 2000 K. The total amount of CPU time was ca. 17 h for each simulation. Maximum step lengths were set at 25° for ϕ and ψ, at 30° for ω and at 0.7° for τ, leading to overall acceptance ratios of 23, 37, 48 and 62% for temperature parameters of 310, 600, 900 and 2000 K, respectively. MMC simulations were also performed for the disaccharides β-D-ManNAc-(1→4)-α-L-Rha **2** and α-D-Glc-(1→3)-α-L-Rha **3**. The temperature parameter was kept at 310 K and 10^6 steps were performed in both cases with the same settings for maximum step lengths as used for **1**. This led to overall acceptance ratios of 53% for **2** and 55% for **3**.

NOEs were calculated from full relaxation matrices **R** which were set up assuming isotropic motion (Boelens et al., 1989; Borgias and James, 1989) and neglecting effects from strong scalar coupling (Kay et al., 1986) and cross-correlation (Bull, 1987; Krishnan and Kumar, 1991). In the case of the global minimum, the relaxation matrix $\mathbf{R}_{Min}$ was based on r^{-6} values with r being proton–proton distances. MMC simulations yielded ensemble average values $< r^{-3} >^2$ (Kessler et al., 1988; Peters et al., 1993; Weimar et al., 1993) which were used to construct an ensemble average relaxation matrix $\mathbf{R}_{MMC}$ as has been described in detail before (Peters et al., 1993). NOEs were calculated from the matrices **R** assuming isotropic motion as published recently (Weimar et al., 1993). A solvent relaxation contribution of 5% was assumed (Bock et al., 1990).

Because of the low molecular weight of trisaccharide **1**, $\omega\tau_c$ must be expected to be close to one. Since NOEs are known to be especially sensitive to τ_c (Isernia et al., 1992), a careful estimation of τ_c was performed on the basis of NOEs which were independent of glycosidic linkage orientations. The intraglycosidic NOEs $H2^M\{H1^M\}$, $H4^M\{H2^M\}$, $H3^M\{H5^M\}$ and $H3^R\{H2^R\}$ were chosen for this purpose. Their experimental NOE curves were compared to theoretical curves from MMC simulations and from the global-minimum conformation A (Table 2). Correlation times were varied in the range 0.22–0.26 ns. A comparison of experimental and theoretical (MMC simulation at 310 K) NOE curves is shown for the NOEs $H3^R\{H2^R\}$ and $H3^M\{H5^M\}$ in Fig. 1 with τ_c set at 0.22, 0.24 and 0.26 ns. From visual inspection, the best fit is obtained for τ_c = 0.24 ns. For a quantitative comparison we calculated 'standard deviations' Δ (Eq. 1, in analogy to 'real' standard deviations) between theoretical and experimental curves:

$$\Delta^2 = N^{-1} \sum_i (e_i - c_i)^2 \qquad (1)$$

with N = number of mixing times τ_m, e_i = experimental NOE enhancement and c_i = theoretical

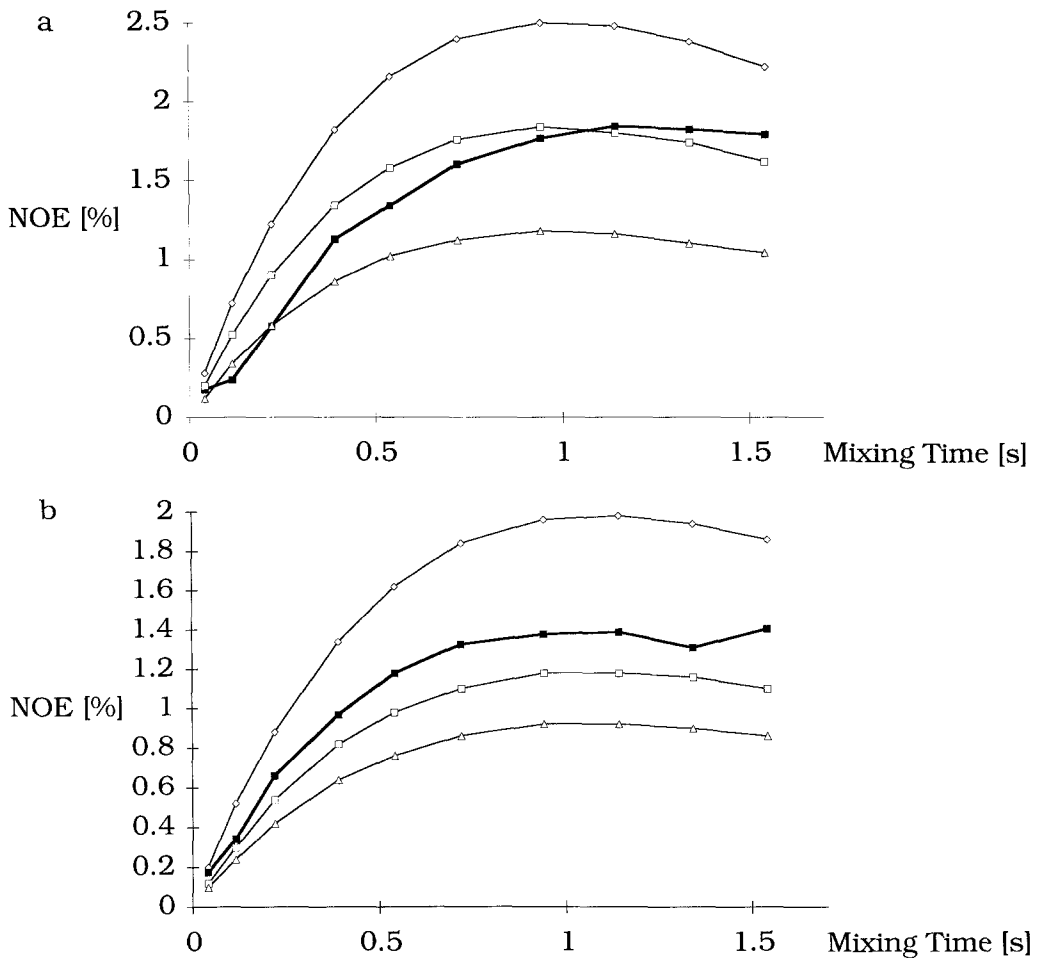

Fig. 1. NOE curves for (a) $H3^{R\alpha}\{H2^{R\alpha}\}$ and (b) $H3^{M}\{H5^{M}\}$ with different settings of the overall motional correlation time τ_c. The temperature parameter was 310 K. Thick lines, filled squares: experimental curves. Thin lines, open symbols: theoretical curves. ◇: τ_c = 0.22 ns; □: τ_c = 0.24 ns; △: τ_c = 0.26 ns.

NOE enhancement. The optimum τ_c value corresponds to the minimum Δ value. It was found that in three cases (NOEs $H4^{M}\{H2^{M}\}$, $H3^{M}\{H5^{M}\}$ and $H3^{R}\{H2^{R}\}$) the optimum value was 0.24 ns, whereas for NOE $H2^{M}\{H1^{M}\}$ an optimum value of 0.25 ns was found. For all further calculations τ_c was chosen to be 0.24 ns. The internal correlation time τ_i for methyl-group rotation was set at 10^{-13} s (Heatley et al., 1980; Brisson and Carver, 1983).

In order to concisely describe flexibility of glycosidic linkages, we introduce entropy-related flexibility parameters. The protocol follows the estimation of internal entropies from systematic grid searches (Carver et al., 1991; Imberty et al., 1993). For a discrete configurational space internal entropy S is defined as:

$$S = -k_b \sum_i p_i \ln p_i \qquad (2)$$

with k_b = Boltzmann constant and p_i = probability of state i. Instead of coarse graining of the continuous configurational space into a discrete configurational space from which entropies can be obtained, we use projections into the individual dimensions as provided by the dihedral angles ϕ, ψ and ω and the glycosidic bond angles τ. These angles can easily be 'classified' by simply dividing the 360° range into N 'classes'. Population distributions are then calculated from the MMC simulations for each dihedral angle with n degrees resolution. A normalised flexibility parameter f is defined in analogy to Eq. 2:

$$f = -(\ln N^{-1})^{-1} \sum_i p_i \ln p_i \quad (3)$$

with i = 1,...,N, N = (360/n) and p_i representing the population in the respective class i. In this work we used N = 360, giving a 1 degree resolution. With Eq. 3 a 'completely rigid' angle, i.e. an angle which resides 100% in one class, leads to a flexibility parameter f of 0. Conversely, with an equal distribution of conformations over the entire 360° range f would be maximally 1.

RESULTS

NMR experiments

Assignment of all ^{1}H NMR resonances of the α- and β-anomers of **1** was straightforward, utilising phase-sensitive TOCSY, COSY and NOESY (Braunschweiler and Ernst, 1983; Marion and Wüthrich, 1983; Bax and Davis, 1985; Davis and Bax, 1985) spectra. ^{1}H NMR chemical-shift values and coupling constants are collected in Table 1. Of course, the effect of the α/β equilibrium is most pronounced for the chemical-shift values of the L-rhamnose protons. No chemical-shift differences for protons of the α- and β-anomers of **1** are detectable for the β-D-ManNAc unit, since these protons are too far from the anomeric centre of the reducing L-rhamnose unit to be influenced directly. The resonance signal of the anomeric proton of $H1^G$ shows a splitting due to

TABLE 1
^{1}H NMR CHEMICAL SHIFTS (PPM) AND COUPLING CONSTANTS (Hz, IN BRACKETS) FOR **1** AS DERIVED FROM A FIRST-ORDER ANALYSIS (303 K, D_2O, 600 MHz)

Residue	H1	H2	H3	H4	H5	H6-*pro-S*	H6-*pro-R*	CH_3-6	NAc
G	5.25 α 5.28 β (3.7)	3.73 (9.8)	3.79 (9.2)	3.61 (9.3)	3.81 (9.9)	3.99–	3.94		
M	5.04 (1.3)	4.66 (4.5)	3.90 (9.8)	3.63 (9.8)	3.50 (10.0)	4.02 (12.6) (2.4)	3.95 (4.3)		2.15 α 2.14 β
Rα	5.24 (2.2)	4.27 (2.8)	4.14 (9.4)	3.99 (9.6)	4.03 (6.5)			1.40	
Rβ	4.94 (< 1.0)	4.29 (3.0)	3.94	3.93	3.58 (6.2)			1.42	

The HDO signal was used as internal reference (δ 4.72 ppm). G = α-D-Glc, M = β-D-ManNAc, R = L-Rha. α and β refer to the configuration of the anomeric centre of L-Rha.

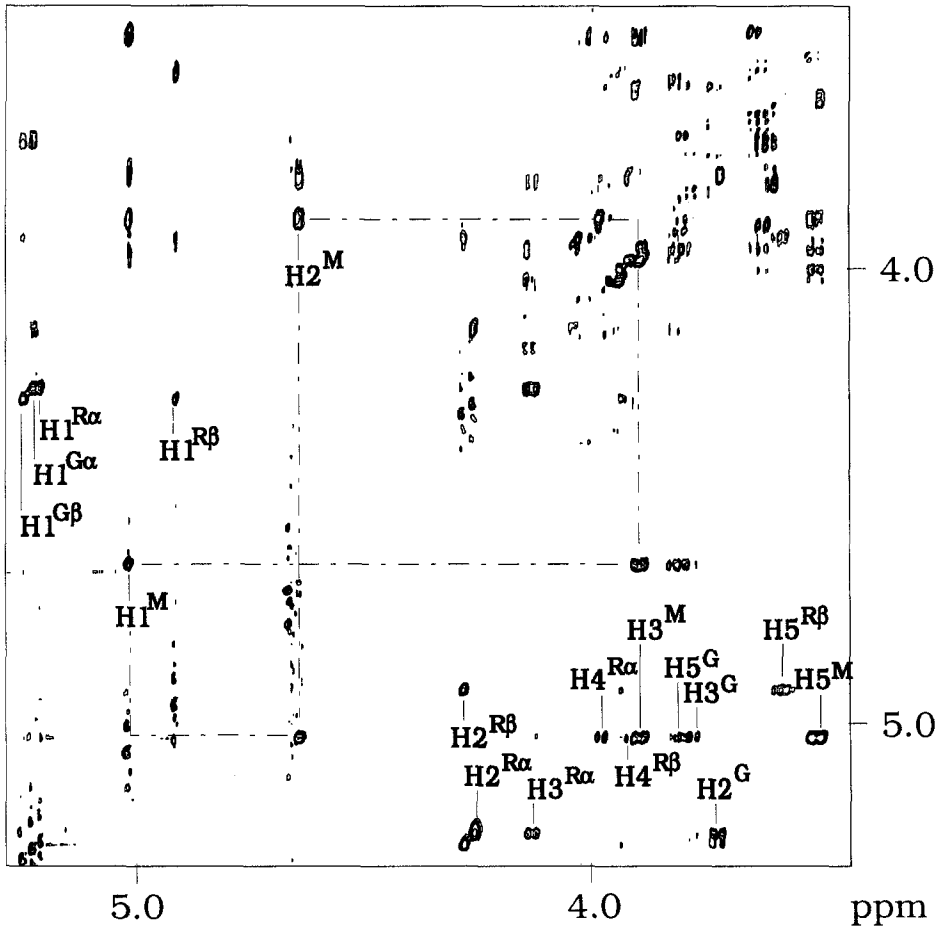

Fig. 2. NOESY spectrum of **1**. The ring-proton region is shown. The mixing time was 900 ms and the 90° hard pulse was 7.5 μs. Data were recorded for 512 t_1 values with 2K data points in t_2. Sixty-four scans were performed for each t_1 value, preceded by four dummy scans. A spectral width of 6 ppm was used in both dimensions. Prior to Fourier transformation, 90° shifted sine-bell weighting functions were applied in both dimensions to give a final data matrix of 2K × 2K data points after zero-filling. To facilitate interpretation of the spectrum we connected dipolar coupling partners $H1^M$ and $H2^M$ as well as $H2^M$ and $H3^M$ with dashed lines, indicating the position of the corresponding diagonal peaks.

the α/β equilibrium (Table 1), indicating a closer proximity of $H1^G$ to the anomeric oxygen of L-rhamnose.

2D NOESY spectra with mixing times from 100 to 900 ms were used to qualitatively identify dipolar contacts between protons. Interglycosidic NOEs are necessary to analyse glycosidic linkage orientations. The NOESY spectrum of **1**, showing the region of the ring protons from 3.4 to 5.4 ppm, is depicted in Fig. 2. The methyl group of the *N*-acetyl residue which lies outside this spectral region does not give rise to any NOE cross peaks. Also, the C6-methyl group of the rhamnose residue does not give rise to any interglycosidic NOEs. Since **1** is a branched saccharide, some protons exhibit NOEs across both glycosidic linkages simultaneously. $H1^M$ is in

close contact with $H4^R$ because of the (1,4) linkage between the two pyranose units, and there is a weak interaction with $H3^R$ as well. Across the (1→3) glycosidic linkage NOEs between $H3^G$ and $H5^G$ are observed (Fig. 2). Similarly, NOE cross peaks are observed between $H2^M$ and the glucose protons $H3^G$ and $H5^G$ (Fig. 2). $H3^R$ is not only in close contact to $H1^G$ and $H5^G$, but also exhibits a small but detectable NOE to $H1^M$. These NOEs should be sensitive to the orientation of *both* glycosidic linkages in **1**. The trace showing NOE cross peaks originating from $H5^M$ does not reveal any interglycosidic contacts. The anomeric proton $H1^G$ of the glucose residue is split into two signals due to α/β isomerisation. The NOE cross-peak patterns of $H1^{G\alpha}$ and $H1^{G\beta}$ are rather similar and allow discrimination between $H3^{R\alpha}$ and $H3^{R\beta}$. Because of spectral overlap with each other and with $H1^{R\alpha}$, these NOEs are unsuitable for a thorough quantitative analysis. Other intraglycosidic NOEs were observed (Fig. 2), but since they do not contain much information about glycosidic linkage orientations, they will not be discussed any further here.

The rigorous quantitative conformational analysis presented here is based on 1D transient NOE spectra, which were acquired utilising Gaussian-shaped (Kessler et al., 1986) 180° pulses for selective inversion. In a first set of experiments NOE curves were measured with mixing times of 750 ms, to identify those resonances for which a quantitative treatment is feasible. Selective irradiation of the anomeric protons of the glucose unit turned out to be rather difficult, not only because of α/β anomerisation, but also because the resonance line of $H1^{R\alpha}$ is too close (Table 1 and Fig. 3). A similar problem arises for the selective inversion of $H2^{R\alpha}$ and $H2^{R\beta}$. Rather long Gaussian pulses (> 400 ms) are required and a quantitative treatment becomes difficult because the initial part of the buildup curve remains unknown. Resonance lines of $H1^M$, $H2^M$, $H5^M$ and $H3^{R\alpha}$ are separated well enough from other signals and allow selective inversion with shorter (80 ms) Gaussian pulses. Selective inversion of these protons yielded accurate NOE curves. The fitting procedure described in Materials and Methods additionally yielded selective spin-lattice relaxation times T_{1sel} (in ms) for the resonances inverted: 748 ($H1^M$), 1160 ($H1^R$), 1214 ($H2^M$), 1154 ($H2^R$), 1123 ($H3^R$) and 1013 ($H5^M$). Altogether, eight interglycosidic NOE curves were measured: $H3^G + H5^G\{H1^M\}$, $H4^R + H3^M\{H1^M\}$, $H3^{R\alpha}\{H1^M\}$, $H3^G + H5^G\{H2^M\}$, $H1^{G\alpha} + H1^{R\alpha}\{H3^{R\alpha}\}$, $H1^{M\alpha}\{H3^{R\alpha}\}$, $H5^{M\alpha}\{H3^{R\alpha}\}$ and $H1^{G\alpha} + H1^{R\alpha}\{H2^{R\alpha}\}$. Figure 3 shows 1D transient NOE spectra obtained from selective inversion of $H1^M$, $H2^M$, $H2^{R\alpha}$ and $H3^{R\alpha}$ to illustrate the general quality of the measurements. Some of the corresponding NOE curves are shown in Fig. 4, together with theoretical curves from energy minimisation and MMC simulations.

Selective inversion of $H1^M$ gives rise to intraglycosidic NOEs of $H2^M$, $H3^M$ and $H5^M$ and interglycosidic NOEs of $H4^R$, $H3^R$, $H3^G$ and $H5^G$. Severe overlap occurs between $H4^R$ and $H3^M$, therefore these two NOEs cannot be integrated separately and the sum of both effects must be used. Since the NOE of $H3^M$ is an intraglycosidic effect, its size should not be influenced by ensemble averaging over glycosidic linkage conformations. Also, $H3^G$ and $H5^G$ cannot be integrated separately, but from 1D transient NOE spectra (Fig. 3) it can be concluded that the NOE of $H3^G$ is approximately twice as large as the one of $H5^G$. $H3^{R\alpha}$ is well separated from other signals, but the corresponding NOE is rather small (0.11% at optimal τ_m!). Nevertheless, a smooth NOE curve could be measured for this interaction. Two of the interglycosidic NOE curves are shown in Figs. 4a ($H3^G + H5^G\{H1^M\}$) and 4b ($H4^R + H3^M\{H1^M\}$). Also, the intraglycosidic NOE curve $H5^M\{H1^M\}$ is shown in Fig. 4c and will be discussed below. For the calculated NOE curves $H4^R + H3^M\{H1^M\}$ (Fig. 4b) it is seen that variation of the temperature parameter in the MMC simulations has a very minor influence, and the MMC-derived curves almost coincide with the

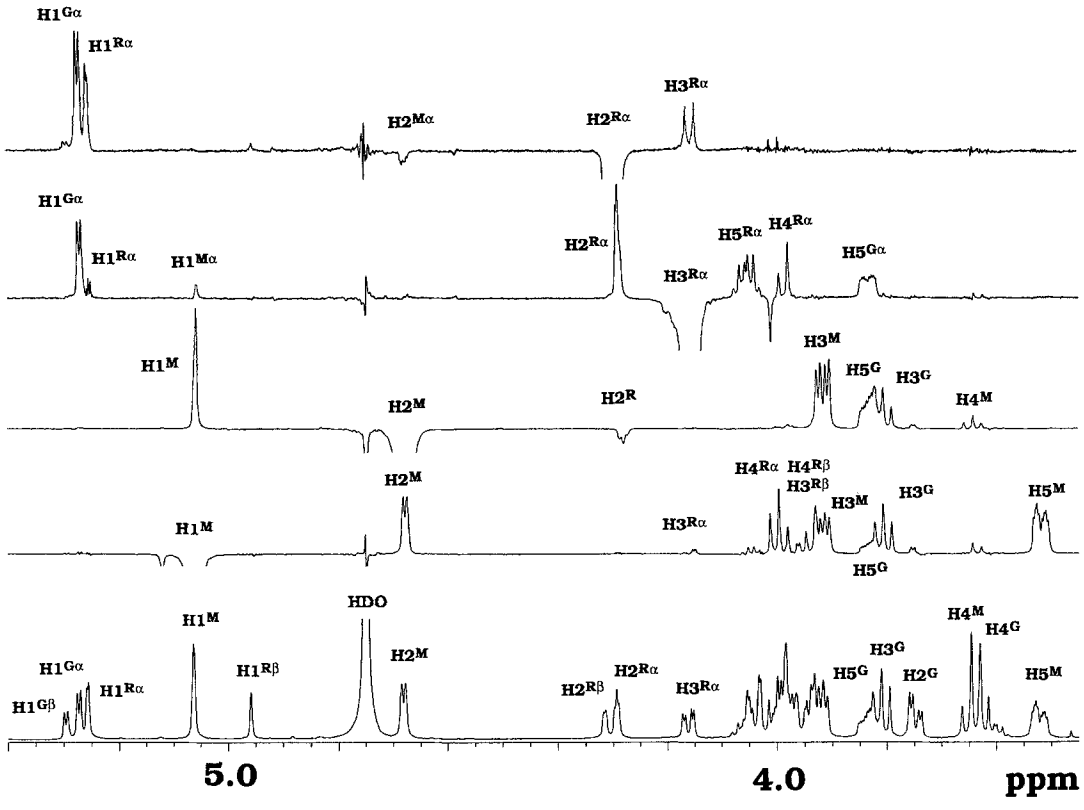

Fig. 3. 1D transient NOE difference spectrum of **1**. The bottom lane shows the ^{1}H NMR spectrum for comparison. The mixing time was 750 ms in all cases. From top to bottom: selective inversion of $H2^{R\alpha}$ (180° Gaussian pulse length: 400 ms); selective inversion of $H3^{R\alpha}$ (180° Gaussian pulse length: 80 ms); selective inversion of $H2^{M}$ (180° Gaussian pulse length: 80 ms); selective inversion of $H1^{M}$ (180° Gaussian pulse length: 80 ms).

one from the minimum-energy calculation. All theoretical curves are a little below the experimental one. The situation is different for the NOE curves of $H3^{G}$ + $H5^{G}\{H1^{M}\}$ (Fig. 4a). The theoretical curves from the minimum-energy calculation and from the MMC simulations at 310 K almost coincide with the experimental NOE curve, whereas the three 'high-temperature' curves are too low, with larger deviations at increasing temperature parameter.

Because of the *N*-acetyl group attached to $C2^{M}$, $H2^{M}$ is shifted out of the ring-proton region and thus provides a perfect target for selective inversion. The curves for the interglycosidic NOEs of $H3^{G}$ and $H5^{G}$ are shown in Fig. 4d, again as a sum of both effects (see above). The experimental NOEs are approximately equal in intensity (estimated from the 1D transient NOE spectrum in Fig. 3). It is immediately obvious that here the theoretical curves from the global-minimum energy conformation and from the MMC simulations at 310 K fit the experimental curve much better than the curves calculated on the basis of MMC simulations at 600, 900 and 2000 K.

$H3^{R\alpha}$ and $H3^{R\beta}$ resonate at different frequencies, but only $H3^{R\alpha}$ can be excited selectively. The major interglycosidic NOE is observed across the (1→3) glycosidic linkage to $H1^{G\alpha}$. Because of spectral overlap, only the sum of $H1^{R\alpha}$ and $H1^{G\alpha}$ can be measured. This is not a problem, because the enhancement of $H1^{R\alpha}$ is almost independent of the conformation of the (1→3) linkage. The

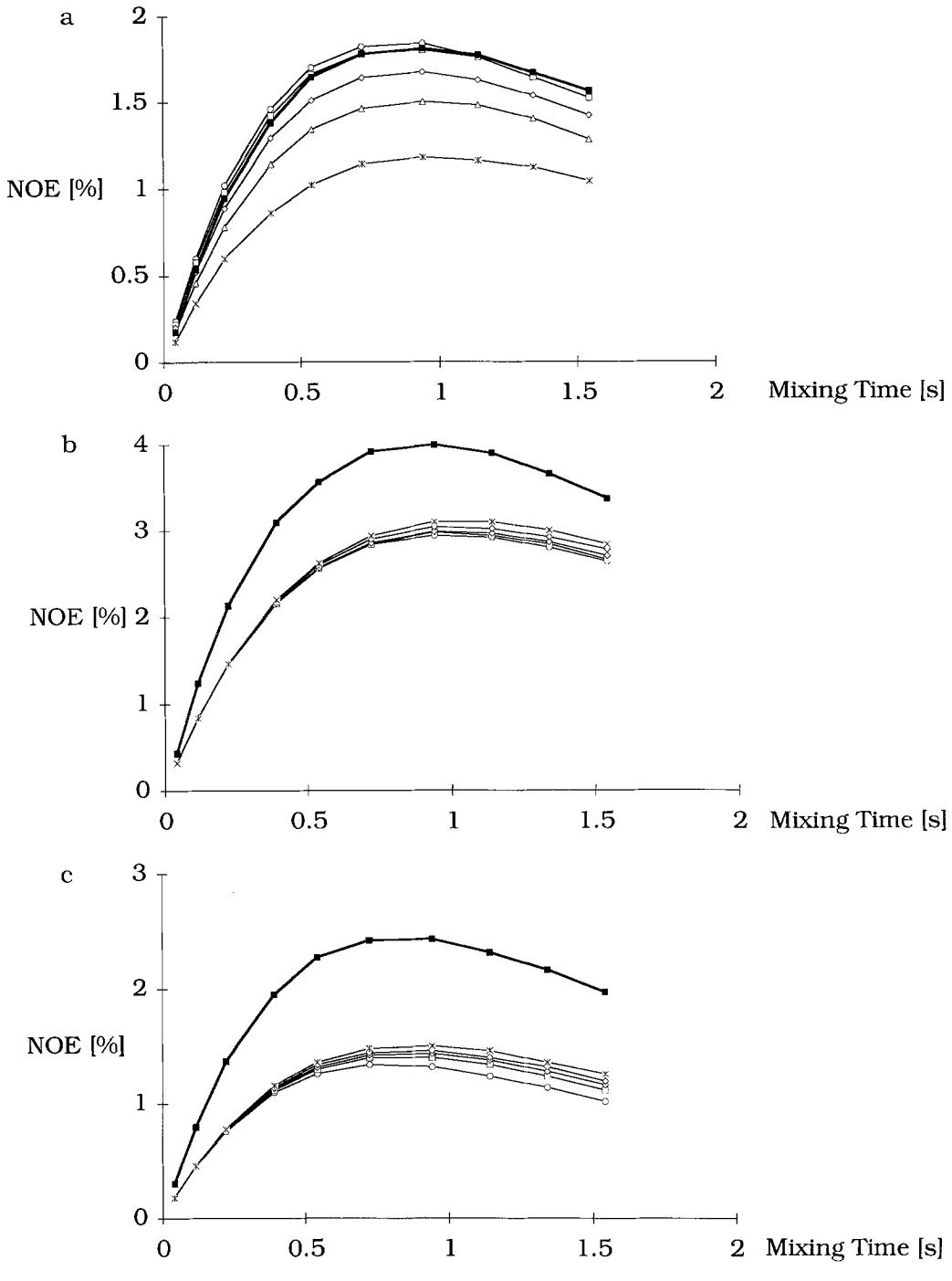

Fig. 4. Experimental and calculated NOE curves. Thick lines with filled square symbols: experimental curves. Open symbols: calculated curves. ○: Minimum A; □: MMC 310 K; ◇: MMC, 600 K; △: MMC 900 K; ✳: MMC 2000 K.

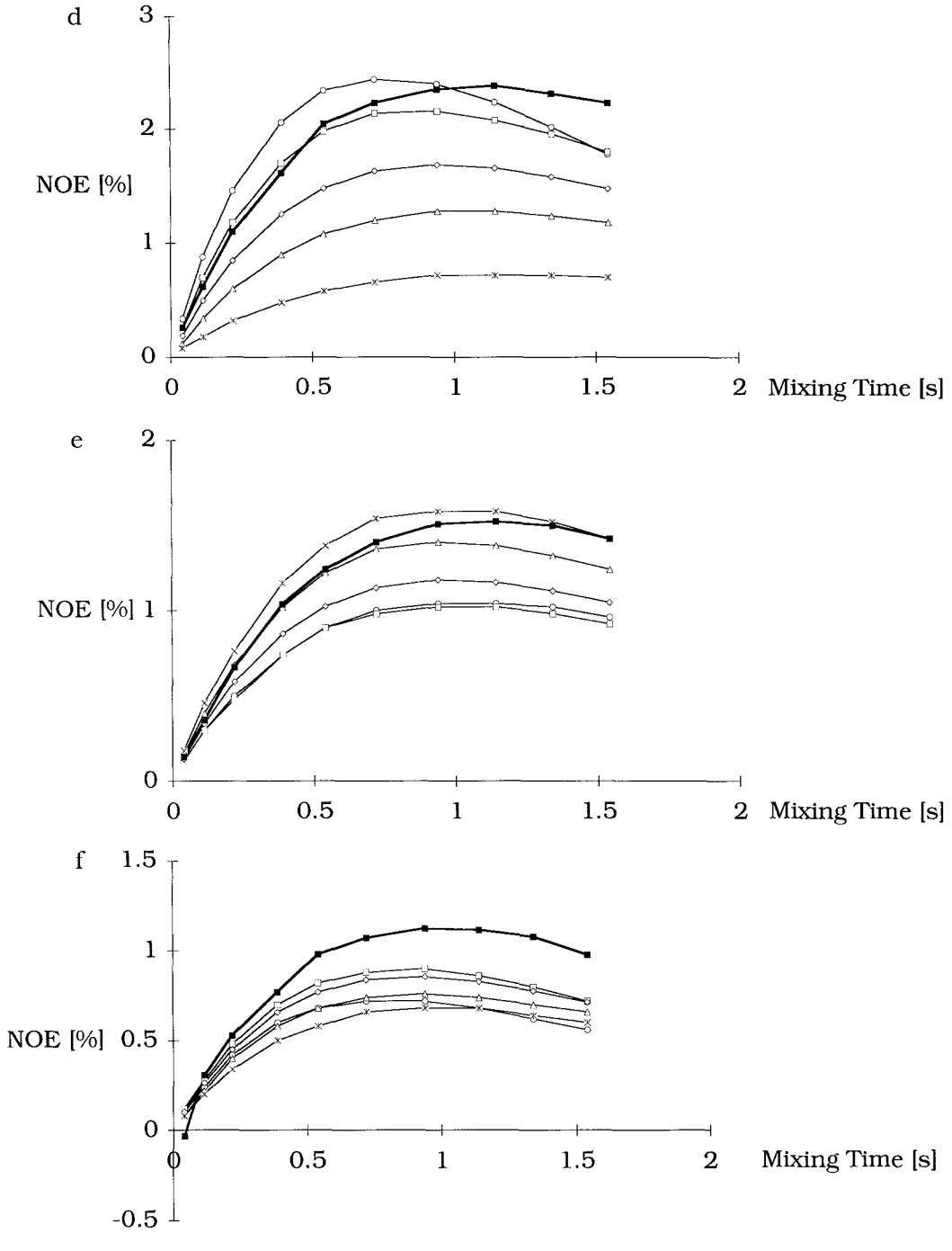

(a) $H3^{G}$ + $H5^{G}\{H1^{M}\}$; (b) $H4^{R}$ + $H3^{M}\{H1^{M}\}$; (c) $H5^{M}\{H1^{M}\}$; (d) $H3^{G}$ + $H5^{G}\{H2^{M}\}$; (e) $H1^{G\alpha}$ + $H1^{R\alpha}\{H3^{R\alpha}\}$; (f) $H5^{G\alpha}\{H3^{R\alpha}\}$.

corresponding experimental NOE curve shows a better fit with curves from MMC simulations at 600, 900 and 2000 K than with curves from the 310 K MMC simulation and from the global minimum A of **1** (Fig. 4e). Another interglycosidic NOE is observed for $H5^{G}$. Here it is seen that the theoretical NOE curve from the MMC simulation at 310 K gives the best fit to the experimental curve (Fig. 4f). An interglycosidic NOE of $H1^{M\alpha}$ is rather small (see above for the opposite NOE $H3^{R\alpha}\{H1^{M}\}$), but again, an NOE curve can be obtained for this effect (data not shown).

It was also possible to selectively excite $H2^{R\alpha}$, resonating rather close to $H2^{R\beta}$ (Fig. 3). A longer 180° pulse was necessary (see experimental part), but fair experimental NOE buildup curves could be obtained (data not shown). There is only one interglycosidic NOE to $H1^{G\alpha}$ which cannot be integrated separately from $H1^{R\alpha}$. A comparison of experimental and calculated curves (data not shown) indicates that variation of the temperature parameter of the MMC simulation has a negligible influence on the shape of the calculated curves.

Apart from the effects described so far, other intraglycosidic NOEs were observed and the corresponding curves were measured. Also, from the decay curves of selectively excited proton signals selective spin-lattice relaxation times were obtained, given in the Materials and Methods section. For all intraglycosidic NOEs only a very minor influence of the temperature parameter used in the MMC simulation was observed and MMC curves were almost identical to those for the minimum-energy conformation A (Table 2).

Finally, we observed a small but notable (< 0.5%) interglycosidic effect of opposite sign. Selective inversion of $H2^{M}$ gave a *negative* enhancement of $H2^{R\alpha}$ (Fig. 3) and, vice versa, selective inversion of $H2^{R\alpha}$ yielded a *negative* enhancement of $H2^{M}$ (Fig. 3). Corresponding NOE curves were obtained (data not shown).

Calculations

The energy minimization of **1** led to a global-minimum conformer A. Two local minima, B and C, with positive values for ϕ and ψ at the $\alpha(1\rightarrow3)$ glycosidic linkage could be found. Their geometries and relative energies are rather similar. Energies and coordinates of the minima are summarized in Table 2. Only the global minimum A was used for a quantitative comparison with the experimental NOE curves, because for local minima B and C, the qualitative differences between theoretical and experimental data were already too large to consider them as potential models for the solution conformational behaviour of **1**. An energy minimization was also performed for a polysaccharide chain containing five trisaccharide units. The global minimum is identical with minimum A. The polysaccharide contains additional $\alpha(1\rightarrow3)$ linkages between the

TABLE 2
RELATIVE ENERGIES AND INTERNAL COORDINATES FOR THE GLOBAL MINIMUM (A) AND THE LOCAL MINIMA (B,C) OF **1**

Minimum	Energy (kcal/mol)	$\phi(1\rightarrow4)$	$\psi(1\rightarrow4)$	$\phi(1\rightarrow3)$	$\psi(1\rightarrow3)$	ω^{G}	ω^{M}
A	0.0	57	10	−58	−32	−61	−66
B	3.8	56	−1	1	30	−60	−66
C	4.5	54	3	13	30	60	−66

Torsion angles are given in degrees.

rhamnose and the *N*-acetyl mannosamine residues. The ϕ and ψ values calculated for these linkages could not be compared to experimental data, because no such $\alpha(1\rightarrow3)$ linkage occurs in **1**. The corresponding calculated values are $\phi = 36°$ and $\psi = 36°$.

MMC simulations were performed as described in the experimental section. The simulation temperature served as a tool to generate different conformation distributions in conformational space. The goal was to identify those NOEs which are sensitive to changes in the conformation distributions at the glycosidic bonds, and on the basis of experimental NOE data assess the amount of flexibility of trisaccharide **1**. The population distributions in Fig. 5 were obtained from MMC simulations of **1** and of the constituent disaccharides **2** and **3**. The plots show that with a temperature parameter of 310 K, there are no transitions between the global minimum A and the local minima B and C (Fig. 5; there is no population of conformational states with positive ϕ or ψ angles at the $(1\rightarrow3)$ linkage). To ensure that it is not the height of the energy barrier between the different minima that prevents transitions, MMC simulations were started from the local minima B and C with the temperature parameter set at 310 K. After approximately 10^3 MMC steps, conformations close to that of the global minimum A were found. Because the relative energies (see above) of the local minima are low enough (Table 2) to allow small but detectable populations of conformers in this part of conformational space, it must be concluded that the lack of transition is of entropic nature (narrow shape of the minima B and C). With temperature parameters set at 600, 900 or 2000 K a significant number of transitions was observed. This is due to the fact that at these temperatures high-energy regions become more 'attractive'.

The population of conformational states at the $(1\rightarrow4)$ linkage in **1** is insensitive to the value of the temperature parameter of the MMC simulation. Also, compared to the conformation distribution calculated for the constituent disaccharide **2** no significant changes can be observed. Thus the orientation of the $(1\rightarrow4)$ linkage is not seriously affected by branching. For the $(1\rightarrow3)$ linkage two effects are immediately obvious. First, the maxima of the ϕ and ψ distribution functions for **1** are shifted towards larger negative ϕ and ψ angles as compared to the constituent disaccharide **3**. Second, with a temperature parameter of 310 K for the MMC simulation of **1**, especially the population distribution of the ψ torsion angle becomes very narrow. This more-or-less qualitative discussion of glycosidic linkage flexibility can be summarised in a very concise fashion. From the population distributions in Fig. 5 flexibility parameters f can be calculated according to Eq. 3. The results are summarised in Table 3 for all MMC simulations of **1** and the constituent disaccharides **2** and **3**. It is immediately obvious that the ψ torsion angle at the $(1\rightarrow3)$ linkage in **1** is most affected by branching. In **1** a value of f = 0.55 is found for a 310 K MMC simulation. This

TABLE 3
FLEXIBILITY PARAMETERS f (EQ. 3) FOR TRISACCHARIDE **1** AND DISACCHARIDES **2** AND **3**

Compound	T (K)	$\phi(1\rightarrow4)$	$\psi(1\rightarrow4)$	$\phi(1\rightarrow3)$	$\psi(1\rightarrow3)$	ω^G	ω^M
1	310	0.60	0.61	0.62	0.55	0.83	0.85
	600	0.66	0.66	0.72	0.66	0.92	0.93
	900	0.69	0.68	0.78	0.74	0.97	0.97
	2000	0.75	0.73	0.83	0.84	0.99	0.99
2	310	0.65	0.63				0.84
3	310			0.66	0.72	0.84	

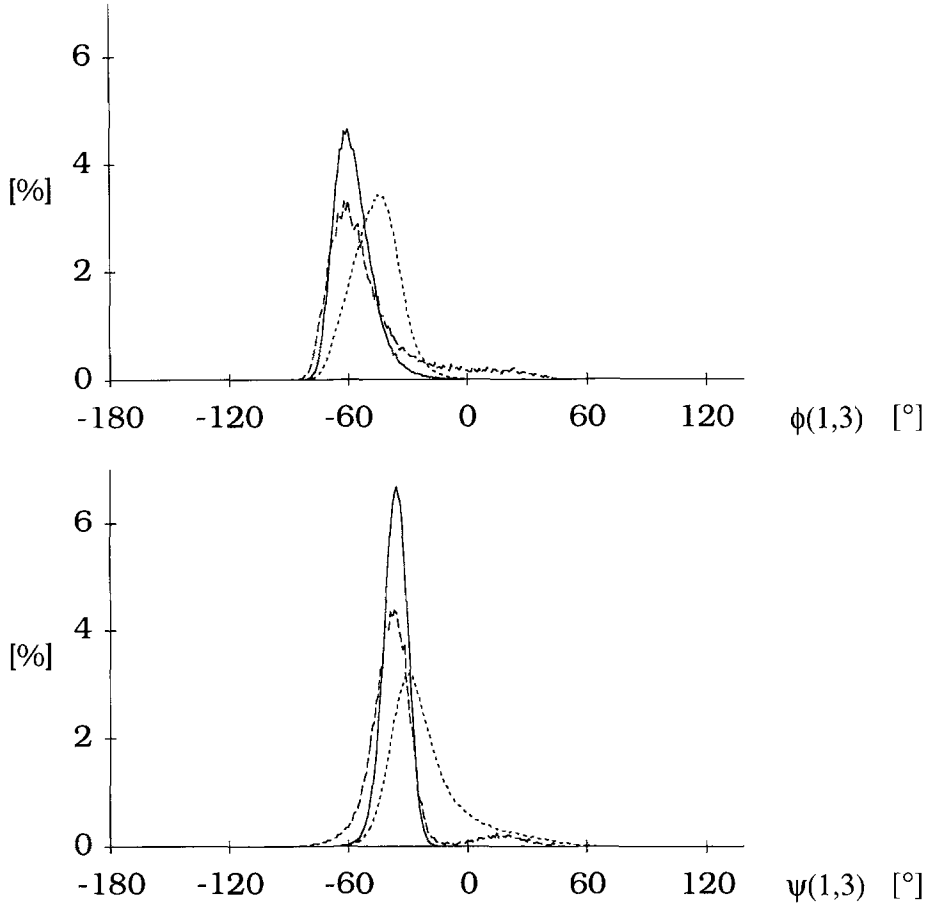

Fig. 5. Population distributions for trisaccharide **1**, calculated from MMC simulations with temperature parameters set at 310 (solid lines) and 600 K (dashed lines). Population distributions for disaccharides **2** and **3** from a 310 K MMC simulation are also shown (dotted lines).

compares to a value of f = 0.72 in **3**. Also, f for the ψ torsion angle at the (1→3) linkage in **1** shows a very pronounced dependence on the temperature parameter of the MMC simulation, covering a range from 0.55 (310 K) to 0.84 (2000 K).

Theoretical NOE curves were calculated from all MMC simulations of **1** and for the global-minimum conformation A. The local minima B and C were not taken into consideration for a quantitative analysis, because a qualitative comparison already showed huge discrepancies between experimental and theoretical NOEs. The interglycosidic NOEs $H3^{G}\{H1^{M}\}$ and $H3^{G}\{H2^{M}\}$ are vanishingly small in conformations B and C, but from Fig. 3 it is seen that these NOEs are of significant size and even larger than the NOEs $H5^{G}\{H1^{M}\}$ and $H5^{G}\{H2^{M}\}$.

DISCUSSION

The calculation of NOE curves critically depends on the choice of the motional correlation time

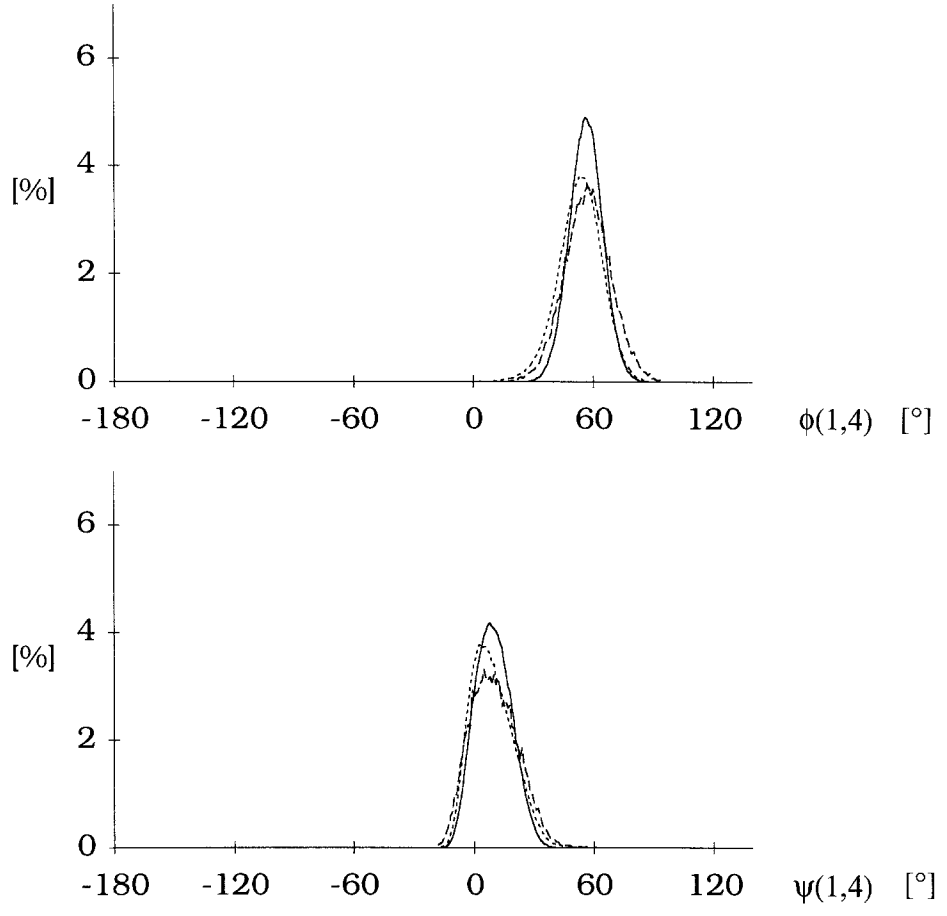

Fig. 5. (continued).

τ_c, because for trisaccharide **1** $\omega\tau_c$ is close to one. Therefore, four intraglycosidic NOEs $H3^R\{H2^R\}$, $H3^M\{H5^M\}$, $H2^M\{H1^M\}$ and $H4^M\{H2^M\}$ were used to determine τ_c. To a good approximation, these NOEs can be assumed to be independent of the distribution of conformers around the glycosidic bonds. The calculation of NOE curves as a function of motional correlation times τ_c yielded a consistent value of $\tau_c = 0.24$ ns, independent of the model used (minimum A or MMC simulations with temperature parameters of 310–2000 K, see also Fig. 1).

The comparison of experimental and theoretical NOE curves shows that only certain interglycosidic NOEs are significantly dependent on the conformation distribution around the glycosidic linkages in **1**. From MMC simulations with different temperature parameters it is seen that the NOEs $H3^G + H5^G\{H1^M\}$ and $H3^G + H5^G\{H2^M\}$ (Figs. 4a and d) are very sensitive to the setting of the temperature parameter and therefore can serve as conformation-distribution sensors. Interestingly, not every interglycosidic NOE can serve as such a sensor, although there is a strong dependence on individual glycosidic-bond conformations in all cases. For instance, the theoretical NOE curves $H4^R + H3^M\{H1^M\}$ (Fig. 4b) are nearly independent of the model (minimum A or any MMC simulation) used.

For a quantitative evaluation of the quality of the fit between experimental and theoretical interglycosidic NOEs, 'standard deviations' Δ were calculated according to Eq. 1 for all interglycosidic NOE curves with a maximum NOE greater than 0.5%. The NOE $H1^{G\alpha}\{H2^{R\alpha}\}$ was not included in this quantitative comparison, because the initial part of the experimental NOE curve is unknown (see above). 'Standard deviations' Δ between experimental and theoretical NOE curves are summarised in Table 4 for the remaining five interglycosidic NOEs. In order to allow an overall comparison, Δ values had to be scaled to account for the absolute size of the corresponding NOEs. This was achieved by taking the sum over the NOEs of each experimental NOE curve and dividing this sum by the number of mixing times used. The values obtained were termed 'average' NOEs (in analogy to 'real' average values) and are also summarised in Table 4. Relative 'standard deviations' Δ_{rel} were then obtained by dividing each Δ value by its corresponding 'average' NOE. Finally, an average relative 'standard deviation' Δ_{av} was calculated and it is seen (Table 4) that the 310 K MMC simulation gave the best overall fit (20% average 'standard deviation') between experimental and theoretical data. Increasing the temperature parameter leads to larger average 'standard deviations'. Even so, it can be argued that the minimum-energy conformation A (Δ_{av} = 25%) and the MMC simulation with a temperature parameter of 600 K (Δ_{av} = 24%) give reasonable results. Very flexible conformational models (MMC simulations with temperature parameters of 900 and 2000 K) for **1** can be excluded with confidence.

The low standard deviations for the 310 K MMC simulation are very satisfying, especially concerning the crude approximations made in the underlying force field. Considering these and other approximations applied, it is not surprising that some of the effects observed are difficult to explain with the model used. These discrepancies are discussed below. At first sight, the negative NOE between $H2^{R\alpha}$ and $H2^{M}$ may indicate an indirect dipolar interaction, often referred to as

TABLE 4
STANDARD DEVIATIONS Δ (EQ. 1) BETWEEN EXPERIMENTAL AND THEORETICAL INTERGLYCOSIDIC NOE BUILDUP CURVES

NOE	Min A	MMC, 310 K	MMC, 600 K	MMC, 900 K	MMC, 2000 K	Average NOE (%)
Δ						
$H3^{G}+H5^{G}\{H1^{M}\}$	0.0531	0.0305	0.1126	0.2479	0.5066	1.3268
$H4^{R}+H3^{M}\{H1^{M}\}$	0.8356	0.8225	0.8093	0.7733	0.7351	2.9289
$H3^{G}+H5^{G}\{H2^{M}\}$	0.2908	0.2187	0.5455	0.8663	1.3074	1.7165
$H1^{R}+H1^{G}\{H3^{R}\}$	0.3591	0.3781	0.2605	0.1000	0.0906	1.0798
$H5^{G}\{H3^{R}\}$	0.3182	0.1877	0.2125	0.2810	0.3439	0.7919
Δ_{rel}						
$H3^{G}+H5^{G}\{H1^{M}\}$	0.04	0.02	0.08	0.19	0.38	
$H4^{R}+H3^{M}\{H1^{M}\}$	0.28	0.28	0.28	0.26	0.25	
$H3^{G}+H5^{G}\{H2^{M}\}$	0.17	0.13	0.32	0.50	0.76	
$H1^{R}+H1^{G}\{H3^{R}\}$	0.33	0.35	0.24	0.09	0.08	
$H5^{G}\{H3^{R}\}$	0.40	0.24	0.27	0.35	0.43	
Δ_{av}	0.25	0.20	0.24	0.28	0.38	

The average NOEs were obtained by summing over individual NOE curves and dividing by the number of mixing times used.

three-spin effect (Neuhaus and Williamson, 1989). Our NOE calculations are based on full relaxation matrices and should reproduce this effect. However, no negative enhancement is predicted. Also, if this negative NOE were due to a three-spin effect, the protons $H2^{R\alpha}$ and $H2^{M}$ should have at least one dipolar coupling partner in common, which they clearly have not (Fig. 3). Therefore, a three-spin effect can be excluded. We feel that an explanation for this effect currently is a matter of speculation and an answer probably will be found performing specific NMR experiments, revealing overall and local motional behaviour of trisaccharide **1**.

For the interglycosidic NOEs $H4^{R}$ + $H3^{M}\{H1^{M}\}$ and $H1^{G\alpha}$ + $H1^{R\alpha}\{H3^{R\alpha}\}$ it was observed that the calculated NOE curves were too low (ca. 30%, compare Table 4) compared to the experimental curves (Figs. 4b and e). In the case of the NOE $H4^{R}$ + $H3^{M}\{H1^{M}\}$ it has to be mentioned that the NOE of $H3^{R\beta}$, which could not be integrated separately, is also included in the experimental curve. However, this NOE should be negligible because it should be smaller than the NOE for $H3^{R\alpha}$ for which an accurate experimental NOE curve could be obtained with a maximum enhancement of 0.11%. A possible explanation for the discrepancies observed is anisotropic tumbling of trisaccharide **1**. This is not unreasonable, because there are examples for anisotropic motion of small saccharides such as cellobiose (Leeflang et al., 1992). Thus, if the proton–proton vectors corresponding to the two interglycosidic NOEs $H4^{R}$ + $H3^{M}\{H1^{M}\}$ and $H1^{G\alpha}$ + $H1^{R\alpha}\{H3^{R\alpha}\}$ are at a significant angle with a preferred axis of reorientation, local reorientation of these vectors will be faster and NOEs will be larger. Indeed, this is the effect observed.

The same argument can be used to explain significant discrepancies between the experimental NOE curves $H5^{M}\{H1^{M}\}$ (Fig. 4c) and $H1^{M}\{H5^{M}\}$ (curves not shown, but they are almost identical with those in Fig. 4c) and their calculated counterparts. These discrepancies are especially noteworthy because they concern intraglycosidic NOEs that are independent of glycosidic linkage orientations in **1**, as seen from the insensitivity of these NOEs towards the temperature parameter used in the MMC simulations (Fig. 4c). Deformation of the pyranose ring is an unlikely explanation for the deviation, because the other intraglycosidic NOEs in the *N*-acetyl mannosamine residue, e.g. $H3^{M}\{H5^{M}\}$ which was used for τ_c calibration, (Fig. 1) show no such discrepancies. Also, a dependency of the size of these NOEs on the rotamer distribution at the $C5^{M}$-$C6^{M}$ bond (relaxation through H6-*pro*-R^{M} and H6-*pro*-S^{M}) can be excluded, because this should result in a significant dependency on the temperature parameter used in the MMC simulation, which is not the case (Fig. 4c). Following our line of argument, it may be conjectured that the vector $H1^{M}$-$H5^{M}$ moves with a correlation time which is different from the overall motional correlation time τ_c. Clearly, if this intraglycosidic NOE were used for calibration of τ_c all other NOEs calculated on this basis would be very different from the experimental values.

CONCLUSIONS

The observation of eight interglycosidic NOEs in **1** a priori greatly restricts the conformational space accessible. Not surprisingly, our study shows that branching results in reduced flexibility, in this case especially a significant restriction of mobility around the ψ torsion angle at the (1→3) linkage in **1** (see Table 3). This is in accordance with conformational analysis studies on other branched saccharides, such as the blood-group determinants (Lemieux et al., 1980; Thøgersen et al., 1982; Bechtel et al., 1990; Yan and Bush, 1990; Mukhopadhyay and Bush, 1991; Cagas and Bush, 1992; Levery et al., 1992; Lin et al., 1992; Miller et al., 1992) and the much debated tissue

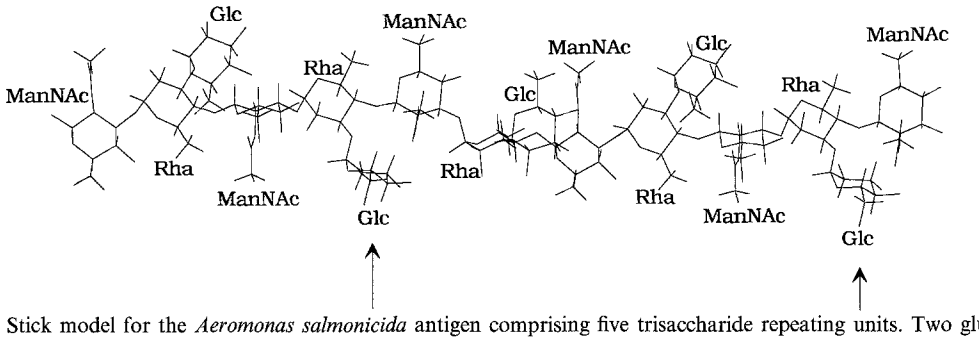

Fig. 6. Stick model for the *Aeromonas salmonicida* antigen comprising five trisaccharide repeating units. Two glucose residues with the same relative orientation towards the helix backbone are indicated with arrows. The model was generated with INSIGHT (Biosym Technologies).

antigen SLe^x which is critically involved in inflammatory response (Hughes, 1992). The *Aeromonas salmonicida* antigen can thus be described as a helical [→3)-ManNAc-(1→4)-Rha(1→] backbone with conformationally restricted glucose residues, winding around the exterior of this helix (Fig. 6). However, a thorough quantitative comparison of experimental and theoretical data showed that flexibility at the glycosidic linkages in **1** cannot be completely neglected. On the whole, our approach, which is based on experimental 1D transient NOE curves and simple MMC simulations, provides a robust tool to study flexibility of glycosidic linkages and to treat gross conformational properties of oligosaccharide epitopes.

On the other hand, our study also reveals shortcomings of currently available methodology. The most important point appears to be the neglect of anisotropy of motion (Lipari and Szabo, 1982a,b; Leeflang et al., 1992). Because for trisaccharide **1** $\omega\tau_c$ is close to one, NOEs are very sensitive to local variations of τ_c (Isernia et al., 1992). In conjunction with other experimental data, such as ROE curves (Isernia et al., 1992; Leeflang and Kroon-Batenburg, 1992) and ^{13}C T_1 and T_2 measurements (Bax, 1991), our NOE data will be very useful for a further detailed study of anisotropic motion of **1**. In combination with such experiments, and on the basis of the data presented here, a more sophisticated theoretical analysis (Brüschweiler et al., 1992) will be possible. Our current efforts aim at scrutinizing more refined theoretical models in order to reproduce the experimental NOE data. One approach is based on relaxed-map MM3 calculations (Weimar, T., Pérez, S., Imberty, A. and Peters, T., manuscript in preparation); a second approach employs MD simulations using a modified GROMOS (Van Gunsteren and Berendsen, 1987) force field (Ott, K.-H., Weimar, T., Meyer, B. and Peters, T., unpublished results).

ACKNOWLEDGEMENTS

We wish to thank the Deutsche Forschungsgemeinschaft for a grant within the Sonderforschungsbereich 169. T.P. thanks NATO for a research grant CRG.890356. Prof. Dr. H. Paulsen (Institute of Organic Chemistry, University of Hamburg) is thanked for the generous gift of a sample of trisaccharide **1**. Prof. Dr. H. Rüterjans (Institute of Biophysical Chemistry, University of Frankfurt) is thanked for giving us access to the computing and NMR facilities in his laboratory. For intense and critical discussions of several aspects of this work we would like

to thank Prof. Dr. B. Meyer, Dr. K.-H. Ott (Complex Carbohydrate Research Center, University of Georgia) and Dr. J.-R. Brisson (National Research Council of Canada, Ottawa).

REFERENCES

Anders, U. (1989) Ph.D. Thesis, University of Frankfurt.
Bax, A. and Davis, D.G. (1985) *J. Magn. Reson.*, **65**, 355–360.
Bax, A. (1991) *Curr. Opin. Struct. Biol.*, **1**, 1030–1035.
Bechtel, B., Wand, A.J., Wroblewski, K., Koprowski, H. and Thurin, J. (1990) *J. Biol. Chem.*, **265**, 2028–2037.
Bock, K., Löhn, H. and Peters, T. (1990) *Carbohydr. Res.*, **198**, 375–380.
Bock, K., Duus, J.Ø., Hindsgaul, O. and Lindh, I. (1992) *Carbohydr. Res.*, **228**, 1–20.
Boelens, R., Koning, T.M.G., Van der Marel, G.A., Van Boom, J.H. and Kaptein, R. (1989) *J. Magn. Reson.*, **82**, 290–308.
Borgias, B.A. and James, T.L. (1989) *Methods Enzymol.*, **176**, 169–183.
Braccini, I., Michon, V., Hervé du Penhoat, C., Imberty, A. and Pérez, S. (1993) *Int. J. Biol. Macromol.*, **15**, 52–55.
Brady, J.W. (1991) *Curr. Opin. Struct. Biol.*, **1**, 711–715.
Braunschweiler, L. and Ernst, R.R. (1983) *J. Magn. Reson.*, **53**, 521–528.
Brisson, J.-R. and Carver, J.P. (1983) *Biochemistry*, **22**, 1362–1368.
Brisson, J.-R., Baumann, H., Imberty, A., Pérez, S. and Jennings, H. (1992) *Biochemistry*, **31**, 4996–5004.
Brüschweiler, R., Roux, B., Blackledge, M., Griesinger, C., Karplus, M. and Ernst, R.R. (1992) *J. Am. Chem. Soc.*, **114**, 2289–2302.
Bull, T.E. (1987) *J. Magn. Reson.*, **72**, 397–413.
Bush, C.A. (1992) *Curr. Opin. Struct. Biol.*, **2**, 655–660.
Cagas, P. and Bush, C.A. (1992) *Biopolymers*, **32**, 277–292.
Carver, J.P. (1991) *Curr. Opin. Struct. Biol.*, **1**, 716–720.
Carver, J.P., Michnik, S.W., Imberty, A. and Cumming, D.A. (1991) *Ciba Found. Symp.*, **158**, 6–26.
Cumming, D.A. and Carver, J.P. (1987a) *Biochemistry*, **26**, 6664–6676.
Cumming, D.A. and Carver, J.P. (1987b) *Biochemistry*, **26**, 6676–6683.
Davis, D.G. and Bax, A. (1985) *J. Am. Chem. Soc.*, **107**, 2820–2821.
Edge, C.J., Singh, U.C., Bazzo, R., Taylor, G.L., Dwek, R.A. and Rademacher, T.W. (1990) *Biochemistry*, **29**, 1971–1974.
Ha, S.N., Madseu, L.J. and Brady, J.W. (1988) *Biopolymers*, **27**, 1927–1952.
Heatley, F., Akhter, L. and Brown, R.T. (1980) *J. Chem. Soc., Perkin II*, 919–924.
Homans, S.W. (1990) *Progr. NMR Spectrosc.*, **22**, 55–81.
Homans, S.W. and Foster, M. (1992) *Glycobiology*, **2**, 143–151.
Hricovíni, M., Shah, R.N. and Carver, J.P. (1992) *Biochemistry*, **31**, 10018–10023.
Hughes, R.C. (1992) *Curr. Opin. Struct. Biol.*, **2**, 687–692.
Imberty, A., Tran, V. and Pérez, S. (1989) *J. Comput. Chem.*, **11**, 205–216.
Imberty, A., Pérez, S., Hricovíni, M., Shah, R.N. and Carver, J.P. (1993) *Int. J. Biol. Macromol.*, **15**, 17–23.
Isernia, C., Paolillo, L., Russo, E., Pastore, A., Zanotti, G. and Macura, S. (1992) *J. Biomol. NMR*, **2**, 573–582.
Jeffrey, G.A., McMullan, R.K. and Takagi, S. (1977) *Acta Crystallogr.*, **B33**, 728–733.
Kay, L.E., Scarsdale, J.N., Hare, D.R. and Prestegard, J.H. (1986) *J. Magn. Reson.*, **68**, 515–525.
Kessler, H., Oschkinat, H. and Griesinger, C. (1986) *J. Magn. Reson.*, **70**, 106–133.
Kessler, H., Griesinger, C., Lautz, J., Müller, A., Van Gunsteren, W.F. and Berendsen, H.J. (1988) *J. Am. Chem. Soc.*, **110**, 3393–3396.
Kessler, H., Mronga, S. and Gemmecker, G. (1991) *Magn. Reson. Chem.*, **29**, 527–557.
Krishnan, V.V. and Kumar, A. (1991) *J. Magn. Reson.*, **92**, 293–311.
Leeflang, B.R. and Kroon-Batenburg, L.M.J. (1992) *J. Biomol. NMR*, **2**, 495–518.
Leeflang, B.R., Vliegenthart, J.F.G., Kroon-Batenburg, L.M.J., Van Eijck, B.P. and Kroon, J. (1992) *Carbohydr. Res.*, **230**, 41–61.
Lemieux, R.U., Bock, K., Delbaere, L.T.J., Koto, S. and Rao, V.S.R. (1980) *Can. J. Chem.*, **58**, 631–653.
Levery, S.B., Holmes, E.H., Harris, D.D. and Hakomori, S. (1992) *Biochemistry*, **31**, 1069–1080.

Levy, S., York, W.S., Stuike-Prill, R., Meyer, B. and Staehelin, L.A. (1991) *Plant J.*, **1**, 195–215.
Lin, Y., Hummel, C.W., Huang, D., Ichikawa, Y., Nicolaou, K.C. and Wong, C. (1992) *J. Am. Chem. Soc.*, **114**, 5452–5454.
Lipari, G. and Szabo, A. (1982a) *J. Am. Chem. Soc.*, **104**, 4546–4559.
Lipari, G. and Szabo, A. (1982b) *J. Am. Chem. Soc.*, **104**, 4559–4570.
Marion, D. and Wüthrich, K. (1983) *Biochem. Biophys. Res. Commun.*, **113**, 967–974.
Meyer, B., Zsiska, M. and Stuike-Prill, R., *Computer Simulation in Condensed Matter, Physics IV*, Springer, Berlin, in press.
Miller, K.E., Mukhopadhyay, C., Cagas, P. and Bush, C.A. (1992) *Biochemistry*, **31**, 6703–6709.
Mukhopadhyay, C. and Bush, C.A. (1991) *Biopolymers*, **31**, 1737–1746.
Neuhaus, D. and Williamson, M. (1989) *The Nuclear Overhauser Effect in Structural and Conformational Analysis*, VCH Publishers, New York, NY, pp. 123–135.
Paulsen, H. and Lorentzen, J.P. (1987) *Carbohydr. Res.*, **165**, 207–227.
Peters, T., Brisson, J.-R. and Bundle, D.R. (1990) *Can. J. Chem.*, **68**, 979–988.
Peters, T., Meyer, B., Stuike-Prill, R., Somorjai, R. and Brisson, J.-R. (1993) *Carbohydr. Res.*, **238**, 49–73.
Poppe, L. and Van Halbeek, H. (1992) *J. Am. Chem. Soc.*, **114**, 1092–1094.
Poppe, L., Stuike-Prill, R., Meyer, B. and Van Halbeek, H. (1992) *J. Biomol. NMR*, **2**, 109–136.
Press, W.H., Flannery, B.P., Teukolsky, S.A. and Vetterling, W.T. (1986) *Numerical Recipes*, Cambridge University Press, Cambridge, pp. 523–528.
Sabesan, S., Duus, J.Ø., Fukunaga, T., Bock, K. and Ludvigsen, S. (1992) *J. Am. Chem. Soc.*, **113**, 3236–3246.
Shaw, D.H., Lee, Y.-Z., Squires, M.J. and Lüderitz, O. (1983) *Eur. J. Biochem.*, **131**, 633–638.
Stuike-Prill, R. and Meyer, B. (1990) *Eur. J. Biochem.*, **194**, 903–919.
Thøgersen, T., Lemieux, R.U., Bock, K. and Meyer, B. (1982) *Can. J. Chem.*, **60**, 44–57.
Tran, V., Buleon, A., Imberty, A. and Pérez, S. (1989) *Biopolymers*, **28**, 679–690.
Van Gunsteren, W.F. and Berendsen, H.J.C. (1987) *Groningen Molecular Simulation (GROMOS) Library Manual*, Biomos, University of Groningen, Groningen.
Weimar, T., Meyer, B. and Peters, T. (1993) *J. Biomol. NMR*, **3**, 399–414.
Widmalm, G., Byrd, R.A. and Egan, W. (1992) *Carbohydr. Res.*, **229**, 195–211.
Winter, W.T., Arnott, S., Isaac, D.H. and Atkins, E.D.T. (1978) *J. Mol. Biol.*, **125**, 1–19.
Yan, Z.Y. and Bush, C.A. (1990) *Biopolymers*, **29**, 799–812.